

Article

Capillary Flow-Based One-Minute Quantification of Amyloid Proteolysis

Taeha Lee ^{1,2} , Da Yeon Cheong ^{1,2}, Kang Hyun Lee ¹, Jae Hyun You ³ , Jinsung Park ^{4,5,6,*}  and Gyudo Lee ^{1,2,*} 

¹ Department of Biotechnology and Bioinformatics, Korea University, Sejong 30019, Republic of Korea; xogk0038@korea.ac.kr (T.L.); 2017270450@korea.ac.kr (D.Y.C.); leoigu97@korea.ac.kr (K.H.L.)

² Interdisciplinary Graduate Program for Artificial Intelligence Smart Convergence Technology, Korea University, Sejong 30019, Republic of Korea

³ Department of Digital Management, Korea University, Sejong 30019, Republic of Korea; hyuni22@korea.ac.kr

⁴ Department of Biomechatronic Engineering, College of Biotechnology and Bioengineering, Sungkyunkwan University, Suwon 16419, Republic of Korea

⁵ Department of MetaBioHealth, Sungkyunkwan University, Suwon 16419, Republic of Korea

⁶ Department of Biopharmaceutical Convergence, Sungkyunkwan University, Suwon 16419, Republic of Korea

* Correspondence: nanojspark@skku.edu (J.P.); lk0807@korea.ac.kr (G.L.)

Abstract: Quantifying the formation and decomposition of amyloid is a crucial issue in the development of new drugs and therapies for treating amyloidosis. The current technologies for grasping amyloid formation and decomposition include fluorescence analysis using thioflavin-T, secondary structure analysis using circular dichroism, and image analysis using atomic force microscopy or transmission electron microscopy. These technologies typically require spectroscopic devices or expensive nanoscale imaging equipment and involve lengthy analysis, which limits the rapid screening of amyloid-degrading drugs. In this study, we introduce a technology for rapidly assessing amyloid decomposition using capillary flow-based paper (CFP). Amyloid solutions exhibit gel-like physical properties due to insoluble denatured polymers, resulting in a shorter flow distance on CFP compared to pure water. Experimental conditions were established to consistently control the flow distance based on a hen-egg-white lysozyme amyloid solution. It was confirmed that as amyloid is decomposed by trypsin, the flow distance increases on the CFP. Our method is highly useful for detecting changes in the gel properties of amyloid solutions within a minute, and we anticipate its use in the rapid, large-scale screening of anti-amyloid agents in the future.

Keywords: capillary; amyloid; lab on paper; hen-egg-white lysozyme; trypsin; autolysis



Citation: Lee, T.; Cheong, D.Y.; Lee, K.H.; You, J.H.; Park, J.; Lee, G. Capillary Flow-Based One-Minute Quantification of Amyloid Proteolysis.

Biosensors **2024**, *14*, 400.

<https://doi.org/10.3390/bios14080400>

Received: 9 July 2024

Revised: 6 August 2024

Accepted: 14 August 2024

Published: 19 August 2024



Copyright: © 2024 by the authors. Licensee MDPI, Basel, Switzerland. This article is an open access article distributed under the terms and conditions of the Creative Commons Attribution (CC BY) license (<https://creativecommons.org/licenses/by/4.0/>).

1. Introduction

The accumulation of amyloids has been extensively researched in the field of medical science for many years, especially in connection with degenerative disorders such as dialysis-related amyloidosis, AL amyloidosis, and Alzheimer's disease [1–5]. These accumulated amyloids, specifically insoluble fibrous aggregates, play a pivotal role in causing damage and functional disabilities in tissues and organs [6–8]. Therefore, understanding the formation and degradation mechanisms of these proteins is a significant concern in biochemical and medical science [9–12]. Comprehensive insights into these proteins have been attained through traditional methods like fluorescence analysis using thioflavin-T, secondary structure analysis via circular dichroism, and advanced imaging techniques such as atomic force microscopy and transmission electron microscopy [13–16]. However, these methods, which require sophisticated spectroscopy or nano-scale imaging equipment and involve considerable analysis time, limit the rapid screening of potential amyloid-degrading drugs.

To address these limitations, paper-based microfluidics, or microfluidic paper-based analytical devices (μ PADs), have emerged as a versatile and cost-effective platform for

various biochemical assays [17–19]. Capillary flow-based paper (CFP), a subtype of μ PADs, has been introduced as a promising alternative [20–22]. This makes them particularly suitable for point-of-care testing and field diagnostics, where simplicity and portability are crucial.

The simplicity and versatility of CFP have been demonstrated in a wide range of applications. For example, Xia et al. developed a CFP material to detect lipase, which is the biomarker for acute pancreatitis [22]. Zhao et al. proposed a CFP-based method for the detection of lipase, which is associated with inflammation, oncogenesis, and allergic reactions [23]. Liu et al. utilized CFP to sense both chymotrypsin and its inhibitors [24]. All of these studies are based on the viscosity changes resulting from alginate, polysaccharide, and gelatin, respectively [22–24]. In detail, the viscosity of a solution inherently can dictate its resistance to capillary flow on CFP [25]. Similar to alginate, polysaccharide, and gelatin, amyloid also has distinct gel-like physical properties as an insoluble denatured polypeptide [26–28]. This similarity suggests that amyloid degradation can be investigated using paper-based microfluidics by monitoring viscosity changes, but this has not been reported so far.

In this study, we investigate the performance of CFP in quantifying amyloid concentration and its proteolysis. Using a hen-egg-white lysozyme amyloid solution as a baseline model, experimental conditions were calibrated to achieve consistent flow-distance measurements. The gel-like physical properties of the amyloid solution result in shorter flow-paths on CFP compared to those in pure water. We observed a significant increase in the flow distance corresponding to amyloid degradation by trypsin. We believe this novel approach holds immense potential and could redefine amyloid analysis methodologies. Additionally, it could significantly accelerate large-scale drug-screening processes, laying the groundwork for future therapeutic innovations.

2. Materials and Methods

2.1. Materials

Hen-egg-white lysozyme (HEWL), trypsin from porcine pancreas, and thioflavin-T (ThT) were sourced from Sigma-Aldrich (St. Louis, MO, USA). Hydrochloric acid (HCl) and sodium hydroxide (NaOH) were obtained from DAEJUNG Chemical & Metals (Seoul, Republic of Korea). Distilled water (DW) and phosphate-buffered saline (PBS, pH 7.4, 1 \times) were obtained from Gibco (West Norriton, PA, USA). Universal indicator paper was acquired from Doosan Scientific (Seoul, Republic of Korea). A membrane syringe filter (0.2 μ m, Whatman GD/X 25) was procured from Cytiva (Marlborough, MA, USA). Polypropylene (PP) film was purchased from Webis (Seoul, Republic of Korea).

2.2. Preparation of HEWL Amyloid

For the formation of HEWL amyloid, HEWL was prepared at a concentration of 10 wt% in DW that had been adjusted to pH 2 using a 1 M HCl solution [29]. This solution was then filtered through a membrane syringe filter (pore size: 0.2 μ m). After filtration, the HEWL solution was transferred into a sterilized vial, sealed, and incubated in an oil bath for 3 days. The resulting HEWL amyloid was neutralized to pH 8 using a 1 M NaOH solution and subsequently diluted with DW (pH 8) to produce amyloids at various concentrations.

2.3. Characterization of the HEWL Amyloid Fibrils

The morphology of the HEWL amyloid fibril was obtained using atomic force microscopy (AFM) (MultiMode VIII, Bruker, Billerica, MA, USA) [30]. For AFM sample preparation, 20 μ L aliquots of the sample were deposited onto freshly cleaved mica, incubated for 5 min, rinsed with 200 μ L of DW, and dried with N₂ gas. ThT assays were conducted using a hybrid multimode reader (Synergy H1, Biotek, Oviedo, FL, USA) at an excitation wavelength of 440 nm and an emission wavelength of 485 nm [31]. The ThT concentration of the reaction solution was adjusted to 20 μ M.

2.4. Trypsin Treatment of HEWL Amyloids

For the proteolytic degradation of HEWL amyloids, trypsin was directly dissolved in the HEWL amyloid solution (Figure 1a). After ensuring homogeneity through vortexing, the mixture was incubated at 37 °C, with mixing performed at 20-min intervals over 2 h. For negative control experiments, thermally denatured trypsin was prepared at 60 °C for 24 h [32].

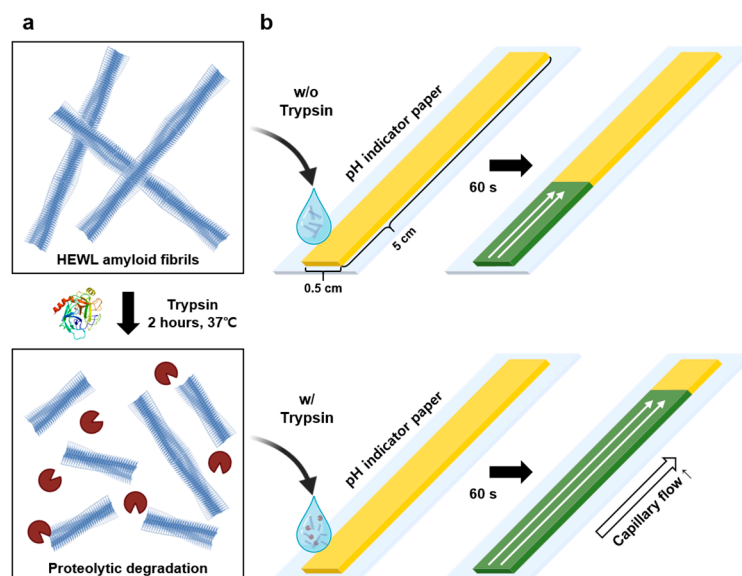


Figure 1. Schematic of (a) HEWL amyloid and its proteolytic degradation by trypsin and (b) comparative analysis of the capillary flow of amyloid solution on CFP treated and untreated with trypsin.

2.5. Fabrication of the CFP

To fabricate CFP, we employed universal pH indicator paper, which is commercially designed for fluid absorption and movement (Figure 1b). The pH indicator paper was trimmed to dimensions of 50 mm × 5 mm (length × width) using a cutting machine. These pieces of pH indicator paper were then affixed to PP film with double-sided tape to ensure precision during experimental procedures. We fabricated an optimal piece of CFP by attaching four pH indicators to a PP film (70 mm × 60 mm), and its optimality was determined using high-resolution images taken with a smartphone camera. We employed a multi-channel pipette (Eppendorf, Hamburg, Germany) to dispense solutions simultaneously onto the CFP.

2.6. Theoretical Background and Data Analysis

Conventionally, capillary action is characterized using the Lucas–Washburn (LW) model (Equation (1)) [33].

$$D_F(t) = \sqrt{\frac{\gamma r \cos \theta}{2\mu}} t \quad (1)$$

Within this formulation, flow distance (D_F) over time describes the progression of a solvent front driven by capillary pressure, and γ symbolizes the surface tension between the liquid and air interfaces. r corresponds to the effective radius of the capillary channel, and θ indicates the contact angle between the liquid phase and the channel. The liquid's viscosity is represented by μ , and t designates the elapsed time. However, the LW equation, originally developed for cylindrical capillaries, assumes a consistent and uninterrupted flow driven purely by capillary forces without accounting for evaporation. In practical applications involving paper-based microfluidics, fluid loss due to evaporation plays a significant role, especially over extended periods and in open systems [34,35]. The porous and hydrophilic nature of paper significantly impacts the corresponding fluid dynamics,

wherein evaporation cannot be neglected. To address these limitations and provide a more accurate description of capillary action in paper-based systems, we used a new expression derived from Darcy's law [36]. This approach allows us to incorporate the effects of evaporation and the unique structural properties of paper, offering a more comprehensive model for fluid movement in these systems. The derived equation is as follows:

$$D_F(t) = \sqrt{\frac{\gamma r \phi h \cos \theta}{4\mu q_0} \left(1 - e^{-\frac{2q_0 t}{\phi h}}\right)} \quad (2)$$

where ϕ is the porosity of the paper, h is the thickness of the porous channel, and q_0 is the evaporation rate defined as the volume of liquid evaporated per unit area and time from the wetted channel. At the limit, that is, the point where there is no evaporation in the channel ($q_0 \rightarrow 0$), this equation reduces to the LW equation.

To achieve a precise quantification of fluid movement on CFP, we captured CFP images using a smartphone (Galaxy S22, Samsung, Suwon-si, Republic of Korea). The D_F was subsequently analyzed using ImageJ software (version 1.54d, NIH). To compute the D_F , the 'solvent front' region pixel value (P_{sf}) of the CFP was divided by the total area pixel value (P_{total}), and this ratio was then multiplied by the CFP's length (L_{CFP} , 50 mm), as shown below.

$$D_F = P_{sf}/P_{total} \times L_{CFP} \quad (3)$$

Through Equation (2), it can be discerned that D_F is inversely proportional to μ . Furthermore, there is direct proportionality between the concentration of trypsin and D_F . Hence, the relationship between D_F , μ , and trypsin concentration can be elucidated as follows:

$$D_F \propto \frac{1}{\sqrt{\mu}} \propto [Trypsin] \quad (4)$$

Based on this theoretical background, we predict that as the concentration of trypsin increases, there is subsequent amyloid degradation, leading to a reduction in the viscosity of the amyloid solution, which, in turn, elevates the D_F .

3. Results

3.1. Morphological and Fluorescent Analysis of HEWL Amyloid Degradation

Previous studies have shown that proteases capable of protein hydrolysis, such as pepsin and trypsin, are effective in degrading amyloid [30,37,38]. Notably, trypsin is known to be able to degrade lysozyme amyloids, which are associated with hereditary lysozyme amyloidosis [37]. Given this background, we utilized AFM and fluorescence analysis to examine the potential degradation of HEWL amyloid by trypsin. In the AFM images, we observed HEWL amyloid fibrils (Figure 2a) and an amyloid fragment formed via trypsin-induced hydrolysis (Figure 2b). As shown in Figure 2a, the AFM images displayed multiple strands of HEWL amyloid fibrils. This amyloid morphology is consistent with AFM images in previous reports [29,30,39–41]. In contrast, the images of the trypsin-treated samples displayed only nanoscale fragments, indicative of degraded amyloids. Along with the morphological comparison of the amyloid samples before and after trypsin treatment, we conducted ThT fluorescence assays to investigate the β -sheet structures within the amyloids. As a result, the ThT fluorescence intensity of the bare amyloid and the trypsin-treated amyloid samples decreased from $19,265 \pm 130$ (mean \pm standard deviation) to $13,639 \pm 191$ (Figure 2c). These findings confirm that trypsin can degrade HEWL amyloids.

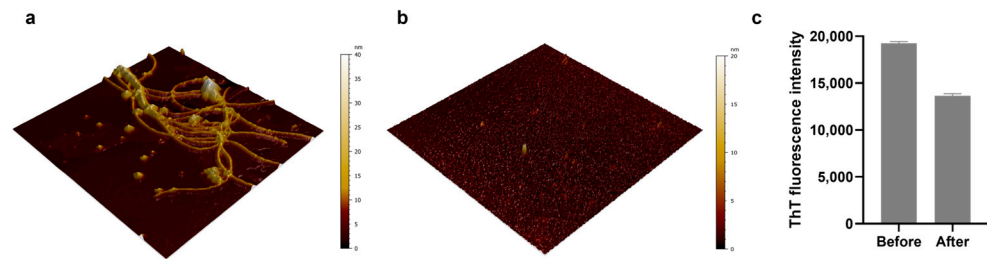


Figure 2. AFM images ($5 \times 5 \mu\text{m}^2$) of (a) HEWL amyloid fibrils and (b) trypsin-treated amyloid sample. (c) ThT fluorescence intensity measurements taken before and after proteolytic degradation by trypsin. The data were obtained through triplicate measurements.

3.2. Development of the CFP Analytical Platform

To effectively evaluate the D_F of the CFP, we designed it such that simultaneous measurement of up to four samples could be performed (Figure 3a). By adopting a systematic approach, we aimed to enhance the accuracy and efficiency of the measurements. Upon completion of the setup, we then proceeded to capture high-resolution images of the pieces of CFP using a readily available smartphone (H.264, AAC, 30 fps), as shown in Figure 3b,c. The smartphone was mounted on a smartphone holder, with the distance between the smartphone and the CFP fixed at 11.5 cm. For subsequent analysis of these images, we used ImageJ software (version 1.54d), a versatile tool known for its robust image-processing capabilities. Specifically, we utilized two plugins, ‘color threshold’ and ‘particle analysis’, which enabled us to differentiate and identify the solvent front area (P_{sf}) as a detection area based on color intensities. We extracted the P_{sf} , which is distinctly represented as the red region in the original images, and subsequently calculated the D_F using Equation (3), as depicted in Figure 3d.

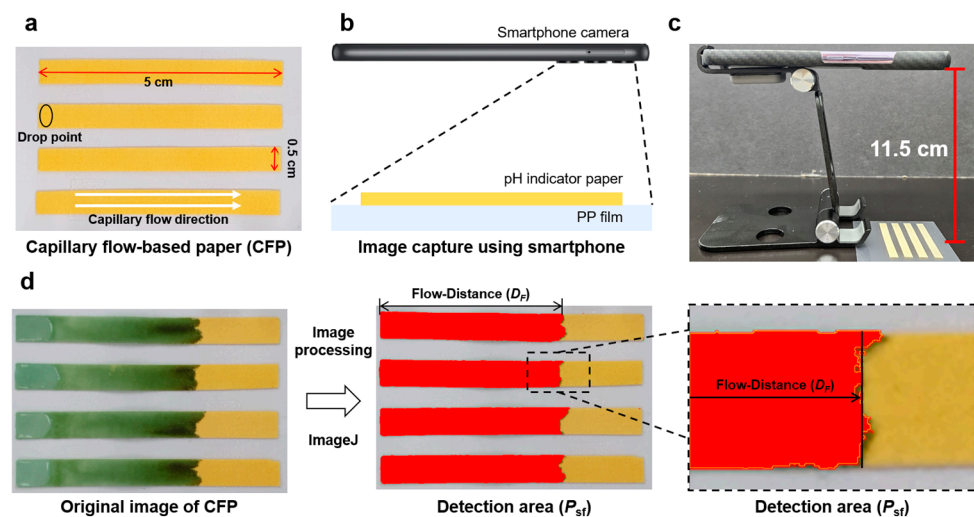


Figure 3. (a) CFP fabricated by attaching four pH indicators to a PP film. Solutions were dispensed at the drop point on the CFP. (b) Schematic illustration and (c) side view of a smartphone mounted on a stand, capturing a piece of CFP from a distance of 11.5 cm. (d) Image-processing procedure used for quantifying the detection area (P_{sf}) on the CFP to accurately calculate the detection factor (D_F).

3.3. CFP Performance for HEWL Amyloid Concentration

To investigate the performance of CFP with respect to amyloid solution, we analyzed the D_F for various concentrations of HEWL amyloid solutions ranging from 0.1 to 10 wt%. Specifically, HEWL solutions (50 μL) were dispensed onto the CFP using a multi-channel pipette. After a duration of 180 s, an image of the CFP was captured, showing that the D_F decreased as the amyloid concentration increased (Figure 4a). This phenomenon can be attributed to the nature of amyloids as insoluble denatured polymers. In detail, as

the amyloid concentration increases, interactions between amyloid fibrils become more prominent, as reflected by a gel-like property [42]. At a certain elevated concentration (5 wt%), the solution of amyloid undergoes a phase transition, shifting from a sol state to a gel state. Meanwhile, the CFP utilized in the experiment turn green at pH values above 8, light green at pH 7, and orange at pH values below 6 [22]. This pH indicator paper not only measures solution pH changes but also provides information about D_F , offering an advantage over traditional colorimetric paper- or hydrogel-based sensors [43–45]. As shown in Figure 4a, a concentration-dependent decrease in pH was observed as the HEWL amyloid was diluted with DW.

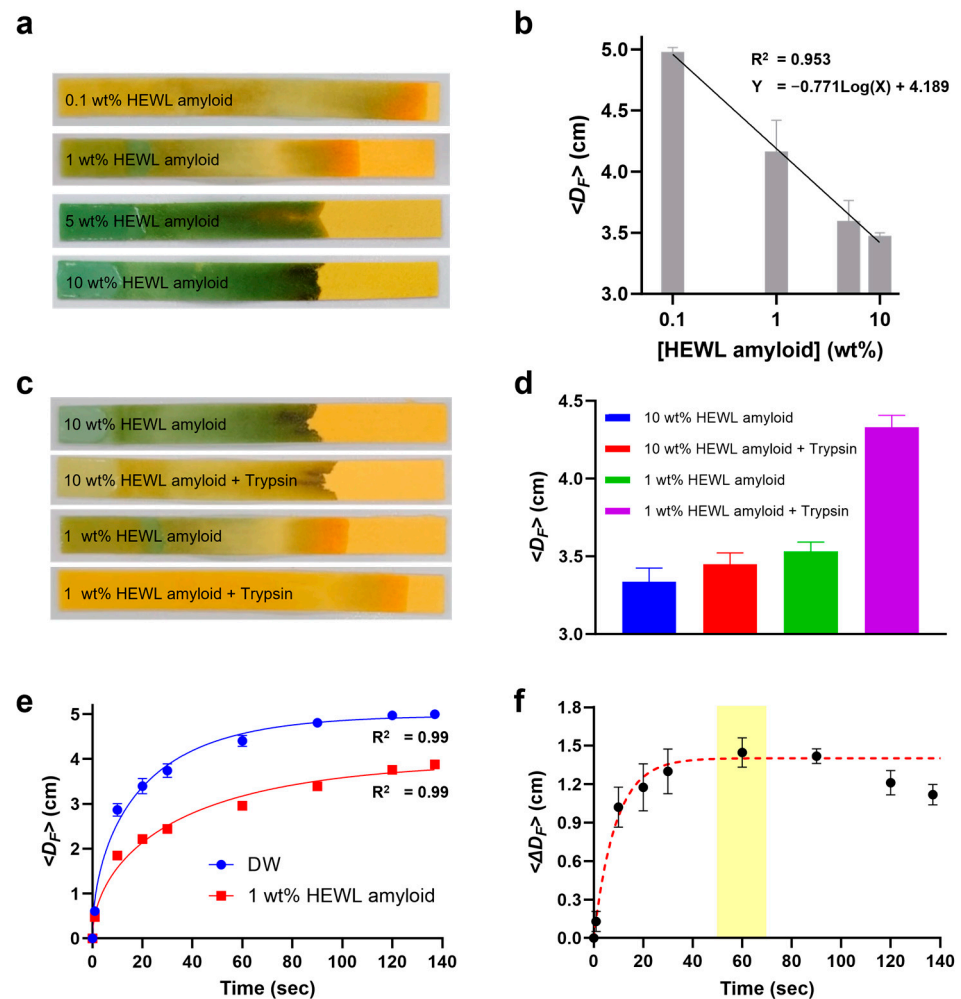


Figure 4. Optimization of the CFP for amyloid solution. (a) Photo of CFP and (b) D_F of different concentrations of HEWL amyloids. (c) Photo of CFP and (d) the D_F between trypsin-treated and untreated HEWL amyloids. (e) Kinetics analysis of 1 wt% HEWL amyloid and DW based on a Darcy-based modified LW model, wherein $D_F(t) = \sqrt{a(1 - e^{bt})}$. (f) A dynamic comparative analysis illustrating the difference in D_F (ΔD_F) between the kinetic curves of DW and 1 wt% amyloid at each timepoint, with the plateau timepoint (60 s) highlighted in yellow.

When plotting D_F against amyloid concentration, an inverse relationship with good linearity ($R^2 = 0.953$) on a logarithmic scale was evident (Figure 4b). The D_F of the 0.1 wt% HEWL amyloid solution almost reached the endpoint of CFP, meaning that the viscosity of the solution was at the DW level. Although the 5 wt% amyloid solution was diluted by half with respect to the original amyloid solution (10 wt%), the D_F between them showed little difference. Consequently, we conducted subsequent experiments using both low-concentration (1 wt%) and high-concentration (10 wt%) HEWL amyloid solutions.

3.4. CFP Test for Trypsin-Treated HEWL Amyloid

CFP tests were performed on the trypsin-treated amyloid solutions, and the D_F values were compared. The HEWL amyloid solutions (1 and 10 wt%) were treated with trypsin (8 mg/mL) and incubated at 37 °C for 2 h. Both the trypsin-treated and untreated amyloid solutions (50 µL) were simultaneously dispensed onto the CFP, and a CFP image was captured after 120 s (Figure 4c). Given the larger gel-to-sol transition, we hypothesized that there would be a more pronounced D_F difference in the 10 wt% amyloid solution after trypsin treatment compared to the 1 wt% solution. However, interestingly, the experimental results (Figure 4d) showed that the D_F difference as a percentile was more noticeable in the 1 wt% amyloid solution (22%) than in the 10 wt% solution (6%). It can be inferred that the 10 wt% amyloid solution maintained a gel-to-gel state, albeit of proteolysis, resulting in minor D_F changes [28]. This is consistent with the negligible difference in D_F observed between the 5 wt% and 10 wt% amyloid solutions, as depicted in Figure 4b. By contrast, the 1 wt% amyloid solution underwent a significant transition from gel to sol [28], resulting in a pronounced change in D_F .

After trypsin treatment, the 10 wt% amyloid solution exhibited a more significant pH drop than the 1 wt% solution (Figure 4c), suggesting enhanced amyloid proteolysis. During proteolysis, the carboxyl groups of amino acids become more numerous owing to peptide bond breakdown, leading to a rise in dissociated hydrogen ions and a subsequent reduction in solution pH [46,47]. Our result implies that while trypsin digested more amyloid in the 10 wt% solution, no gel-to-sol phase transition happened. This phenomenon underscores the importance of amyloid density when evaluating amyloid proteolysis using CFP. Thus, we adopted 1 wt% HEWL amyloid solution as an optimal condition for further experiments with CFP.

3.5. CFP Kinetics for Optimization of Analysis Time

To delve deeper into comprehending the capillary action of amyloid solutions in CFP, we embarked on a series of kinetics analyses. We used a 1 wt% amyloid solution for these analyses, and hypothesizing that there would be complete degradation of amyloid, we employed DW as a negative control for a comparative study (Figure 4e). The D_F for both solutions increased over time, and DW exhibited a higher D_F rate than the amyloid solution, as expected. A significant observation was the steep initial increase in the kinetics curves for both fluids, transitioning to a more gradual ascent post 10 s. This phenomenon is attributed to capillary action, as the solution is rapidly drawn into the nano-porous structure of CFP and gradually transitions to a steady state [48]. Our results do not conform to the conventional LW model but rather match better with the modified LW model using Darcy's law. The data were fit to the following equation:

$$D_F(t) = \sqrt{a(1 - e^{bt})} \quad (5)$$

The parameter a is given by the following equation:

$$a = \frac{\gamma r \phi h \cos \theta}{4 \mu q_0} \quad (6)$$

The parameter b is expressed as follows:

$$b = \frac{2q_0}{\phi h} \quad (7)$$

We found that the optimal fitting values for DW are $a = 24.73$ and $b = 0.03$, while for HEWL, the optimal fitting values are $a = 15.58$ and $b = 0.02$. This equation (Equation (5)) models the growth pattern of the D_F ; here, a represents the asymptotic maximum value of D_F , and b represents the rate at which the D_F approaches its maximum. The use of this model allows for capturing the nonlinear dynamics observed in the experiments

more accurately. Calculating q_0 based on a could lead to inaccuracies due to the potential variability in the asymptotic maximum values, which may be influenced by external factors. Therefore, we used the parameter b to calculate q_0 as it directly reflects the evaporation rate. Although there are no exact studies analyzing the porosity and height of the CFP we used, the porosity (ϕ) of similar filters is known to be approximately 0.6, and the thickness (h) is approximately 220 μm [49]. Based on this, we calculated the evaporation rates (q_0) as follows: for DW, $q_0 \approx 1.94 \mu\text{m/s}$, and for HEWL, $q_0 \approx 1.09 \mu\text{m/s}$. These values indicate that DW has a higher evaporation rate compared to the amyloid solution, which aligns with our observations of the D_F rates. This suggests that the higher viscosity and gel-like properties of the amyloid solution result in a slower evaporation rate, thus impacting the capillary flow dynamics in the CFP system. Additionally, by applying the modified LW equation, the fit accuracy for the D_F of the DW and HEWL improved significantly ($R^2 = 0.99$).

The new model derived from Darcy's law provided more accurate predictions by accounting for fluid loss due to evaporation. This model effectively explained the nonlinear kinetics observed in the experiments, particularly reflecting the characteristic transition from an initial steep increase to a gradual one. This study demonstrates that the modified model applying Darcy's law can more precisely describe capillary action in the CFP system, suggesting that this approach could be useful for analyzing various biological materials.

To determine the optimal analysis time for CFP, a dynamic comparative analysis was conducted by calculating ΔD_F through the subtraction of the two kinetic curves presented in Figure 4e. The ΔD_F continued to increase for 30 s and then reached saturation; then, it gradually decreased after 60 s (Figure 4f). This behavior is due to the potential energy of capillary action decreasing as the solution moves toward the CFP's endpoint (50 mm). Excluding two data points post 100 s and applying an exponential fit yielded a robust correlation ($R^2 = 0.96$). We confirmed that the minimum time point at which the plateau becomes apparent is 60 s, and, consequently, we have determined that this time-point is the optimal analysis time for conducting amyloid experiments based on CFP.

3.6. CFP-Based Quantification of Amyloid Degradation

We investigated the quantification of amyloid degradation by trypsin using CFP, employing the optimal conditions determined in previous experiments: HEWL amyloid concentration (1 wt%) and analysis time (60 s). Amyloid proteolysis was tested across 12 different trypsin concentration conditions ranging from 1 to 40 mg/mL, and the D_F value was quantified through CFP analysis. Figure 5a indicates that as the trypsin concentration increased in 1 mg/mL intervals, a gradual expansion in the solvent-front was observed. Notably, CFP seems to show poor performance at high trypsin concentrations (>8 mg/mL). To analyze this phenomenon in detail, the D_F was calculated and plotted against trypsin concentration (Figure 5b). D_F increased proportionally with trypsin concentration, with a pronounced linearity observed within the concentration range of 1 to 8 mg/mL. Through an analysis of the proteolysis effect of trypsin on a 1% HEWL amyloid solution (pH 8 and 37 °C), the LOD and sensitivity values were determined to be 2 mg/mL and 2.07 mm·L/g, respectively. This indicates that the extent of amyloid hydrolysis by trypsin can be precisely analyzed using CFP. However, beyond a certain trypsin concentration (>8 mg/mL), a drastic decline of approximately 35% in the D_F was observed. This phenomenon is attributed to trypsin autolysis or potential distortion of the protein molecule due to high trypsin concentrations [50], and it does not reflect an issue with CFP itself. These findings suggest that CFP not only facilitates easy analysis of amyloid proteolysis but also enables the determination of the appropriate protease concentration for analysis.

To validate whether the degradation of HEWL amyloid was genuinely due to the activity of trypsin, we examined the hydrolysis of amyloid by thermally denatured trypsin. To ensure robust experiments, we adopted a trypsin concentration of 8 mg/mL, which appeared to induce the highest amyloid degradation under our experimental conditions. As shown in Figure 6, the denatured trypsin did not induce amyloid degradation at all

compared to the negative control (amyloid only). As a result, it was concluded that the observed D_F change in CFP could indeed be attributed to amyloid degradation by trypsin.

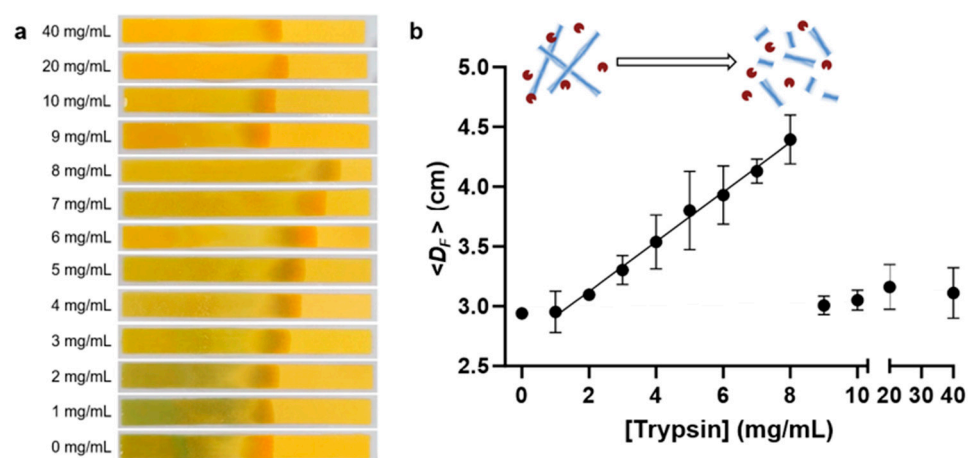


Figure 5. CFP-based quantification of amyloid proteolysis by trypsin. (a) Photo of CFP and (b) the calculated D_F against trypsin concentration (0 to 40 mg/mL). The data were obtained through triplicate measurements (mean \pm standard deviation).

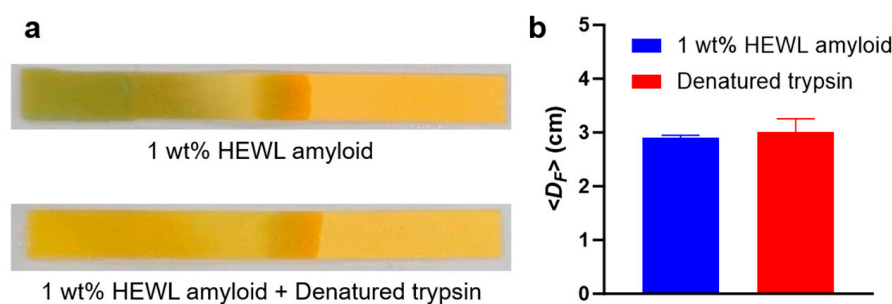


Figure 6. (a) Photo of CFP and (b) the calculated D_F for HEWL amyloids with and without inactivated trypsin. The data were obtained through triplicate measurements (mean \pm standard deviation).

4. Conclusions

In this study, we introduced capillary flow-based paper (CFP) as a fast and efficient method for quantifying amyloid degradation, addressing the challenges associated with existing techniques that require complex equipment and extensive analysis times. The amyloid solution exhibits gel-like properties, leading to a distinctive flow-distance (D_F) pattern within CFP. Through the analysis of D_F concerning amyloid concentration, the investigation of D_F and pH changes resulting from amyloid hydrolysis, and kinetic analyses, we determined the optimal amyloid concentration and analysis time for CFP experiments. We demonstrated that CFP can be utilized to analyze the extent of protease-induced amyloid hydrolysis. Furthermore, we confirmed that CFP is an effective tool for exploring the protease concentration range that yields the best performance in amyloid hydrolysis. Our CFP-based analytical method will facilitate the screening for amyloid inhibitors or degraders and suggest an optimal concentration range. We emphasize the potential of CFP as an excellent alternative technology capable of saving both time and resources in amyloid research. While our current study focused on purified amyloids, future work will explore the application of CFP to various biological fluids to enhance its accuracy and applicability in amyloid drug-screening evaluations.

Author Contributions: This manuscript was written with contributions from all the authors. Methodology, D.Y.C. and K.H.L.; Software, D.Y.C. and J.H.Y.; Validation, T.L.; Formal analysis, D.Y.C.; Investigation, K.H.L. and J.H.Y.; Data curation, K.H.L. and J.H.Y.; Writing—original draft, T.L.; Writing—review & editing, J.P. and G.L.; Visualization, G.L.; Supervision, J.P. and G.L. All authors have read and agreed to the published version of the manuscript.

Funding: This research received no external funding.

Institutional Review Board Statement: Not applicable.

Informed Consent Statement: Not applicable.

Data Availability Statement: The original contributions presented in the study are included in the article, further inquiries can be directed to the corresponding authors.

Acknowledgments: This study was supported by the National Research Foundation of South Korea (NRF) under Grant No. NRF-2023R1A2C2004964 and RS-2024-00438542. This work was also supported by the Ministry of Health and Welfare (KH140292) and the Ministry of Science and ICT (IITP-2024-RS-2023-00258971). This study was also sponsored by a Korea University Grant and the BK21 FOUR (Fostering Out-standing Universities for Research).

Conflicts of Interest: The authors declare no conflicts of interest.

References

1. Caughey, B.; Peter, J.; Lansbury, P.T. Protofibrils, Pores, Fibrils, and Neurodegeneration: Separating the Responsible Protein Aggregates from The Innocent Bystanders. *Annu. Rev. Neurosci.* **2003**, *26*, 267–298. [[CrossRef](#)]
2. Chiti, F.; Dobson, C.M. Amyloid formation by globular proteins under native conditions. *Nat. Chem. Biol.* **2009**, *5*, 15–22. [[CrossRef](#)] [[PubMed](#)]
3. Gouras, G.K.; Tampellini, D.; Takahashi, R.H.; Capetillo-Zarate, E. Intraneuronal β -amyloid accumulation and synapse pathology in Alzheimer's disease. *Acta Neuropathol.* **2010**, *119*, 523–541. [[CrossRef](#)]
4. Hardy, J.A.; Higgins, G.A. Alzheimer's Disease: The Amyloid Cascade Hypothesis. *Science* **1992**, *256*, 184–185. [[CrossRef](#)] [[PubMed](#)]
5. Merlini, G.; Bellotti, V. Molecular Mechanisms of Amyloidosis. *N. Engl. J. Med.* **2003**, *349*, 583–596. [[CrossRef](#)]
6. Cho, D.-H.; Nakamura, T.; Fang, J.; Cieplak, P.; Godzik, A.; Gu, Z.; Lipton, S.A. S-Nitrosylation of Drp1 Mediates β -Amyloid-Related Mitochondrial Fission and Neuronal Injury. *Science* **2009**, *324*, 102–105. [[CrossRef](#)]
7. Head, E.; Doran, E.; Nistor, M.; Hill, M.; Schmitt, F.A.; Haier, R.J.; Lott, I.T. Plasma Amyloid- β as a Function of Age, Level of Intellectual Disability, and Presence of Dementia in Down Syndrome. *J. Alzheimers Dis.* **2011**, *23*, 399–409. [[CrossRef](#)] [[PubMed](#)]
8. Milani, P.; Basset, M.; Russo, F.; Foli, A.; Palladini, G.; Merlini, G. The lung in amyloidosis. *Eur. Respir. Rev.* **2017**, *26*, 170046. [[CrossRef](#)]
9. Knowles, T.P.J.; Vendruscolo, M.; Dobson, C.M. The amyloid state and its association with protein misfolding diseases. *Nat. Rev. Mol. Cell Biol.* **2014**, *15*, 384–396. [[CrossRef](#)]
10. Friedrich, R.P.; Tepper, K.; Rönicke, R.; Soom, M.; Westermann, M.; Reymann, K.; Kaether, C.; Fändrich, M. Mechanism of amyloid plaque formation suggests an intracellular basis of A β pathogenicity. *Proc. Natl. Acad. Sci. USA* **2010**, *107*, 1942–1947. [[CrossRef](#)]
11. Eckman, E.A.; Reed, D.K.; Eckman, C.B. Degradation of the Alzheimer's amyloid beta peptide by endothelin-converting enzyme. *J. Biol. Chem.* **2001**, *276*, 24540–24548. [[CrossRef](#)] [[PubMed](#)]
12. Lee, D.; Park, D.; Kim, I.; Lee, S.W.; Lee, W.; Hwang, K.S.; Lee, J.H.; Lee, G.; Yoon, D.S. Plasmonic nanoparticle amyloid corona for screening A β oligomeric aggregate-degrading drugs. *Nat. Commun.* **2021**, *12*, 639. [[CrossRef](#)]
13. Biancalana, M.; Koide, S. Molecular mechanism of Thioflavin-T binding to amyloid fibrils. *Biochim. Et Biophys. Acta (BBA)-Proteins Proteom.* **2010**, *1804*, 1405–1412. [[CrossRef](#)] [[PubMed](#)]
14. Arosio, P.; Knowles, T.P.J.; Linse, S. On the lag phase in amyloid fibril formation. *Phys. Chem. Chem. Phys.* **2015**, *17*, 7606–7618. [[CrossRef](#)] [[PubMed](#)]
15. Adamcik, J.; Mezzenga, R. Study of amyloid fibrils via atomic force microscopy. *Curr. Opin. Colloid Interface Sci.* **2012**, *17*, 369–376. [[CrossRef](#)]
16. Galzitskaya, O.V.; Selivanova, O.M.; Gorbunova, E.Y.; Mustaeva, L.G.; Azev, V.N.; Surin, A.K. Mechanism of Amyloid Gel Formation by Several Short Amyloidogenic Peptides. *Nanomaterials* **2021**, *11*, 3129. [[CrossRef](#)]
17. Martinez, A.W.; Phillips, S.T.; Whitesides, G.M. Three-dimensional microfluidic devices fabricated in layered paper and tape. *Proc. Natl. Acad. Sci. USA* **2008**, *105*, 19606–19611. [[CrossRef](#)]
18. Lisowski, P.; Zarzycki, P.K. Microfluidic Paper-Based Analytical Devices (μ PADs) and Micro Total Analysis Systems (μ TAS): Development, Applications and Future Trends. *Chromatographia* **2013**, *76*, 1201–1214. [[CrossRef](#)]
19. Morbioli, G.G.; Mazzu-Nascimento, T.; Stockton, A.M.; Carrilho, E. Technical aspects and challenges of colorimetric detection with microfluidic paper-based analytical devices (μ PADs)—A review. *Anal. Chim. Acta* **2017**, *970*, 1–22. [[CrossRef](#)]

20. Ulep, T.-H.; Zenhausem, R.; Gonzales, A.; Knoff, D.S.; Lengerke Diaz, P.A.; Castro, J.E.; Yoon, J.-Y. Smartphone based on-chip fluorescence imaging and capillary flow velocity measurement for detecting ROR1+ cancer cells from buffy coat blood samples on dual-layer paper microfluidic chip. *Biosens. Bioelectron.* **2020**, *153*, 112042. [[CrossRef](#)]
21. Songok, J.; Toivakka, M. Enhancing Capillary-Driven Flow for Paper-Based Microfluidic Channels. *ACS Appl. Mater. Interfaces* **2016**, *8*, 30523–30530. [[CrossRef](#)]
22. Xia, S.; Yin, F.; Xu, L.; Zhao, B.; Wu, W.; Ma, Y.; Lin, J.-M.; Liu, Y.; Zhao, M.; Hu, Q. Paper-Based Distance Sensor for the Detection of Lipase via a Phase Separation-Induced Viscosity Change. *Anal. Chem.* **2022**, *94*, 17055–17062. [[CrossRef](#)] [[PubMed](#)]
23. Zhao, B.; Qi, L.; Tai, W.; Zhao, M.; Chen, X.; Yu, L.; Shi, J.; Wang, X.; Lin, J.-M.; Hu, Q. Paper-Based Flow Sensor for the Detection of Hyaluronidase via an Enzyme Hydrolysis-Induced Viscosity Change in a Polymer Solution. *Anal. Chem.* **2022**, *94*, 4643–4649. [[CrossRef](#)]
24. Liu, S.; Wang, X.; Hu, Q.Z.; Geng, Y.; Dong, H. Paper-based flow sensor for detection of chymotrypsin and its inhibitors via viscosity change of gelatin. *J. Food Compos. Anal.* **2023**, *116*, 105064. [[CrossRef](#)]
25. Miller, E.E.; Miller, R.D. Physical Theory for Capillary Flow Phenomena. *J. Appl. Phys.* **2004**, *27*, 324–332. [[CrossRef](#)]
26. Zhou, X.-M.; Shimanovich, U.; Herling, T.W.; Wu, S.; Dobson, C.M.; Knowles, T.P.J.; Perrett, S. Enzymatically Active Microgels from Self-Assembling Protein Nanofibrils for Microflow Chemistry. *ACS Nano* **2015**, *9*, 5772–5781. [[CrossRef](#)]
27. Xu, Z.; Shan, G.; Hao, N.; Li, L.; Lan, T.; Dong, Y.; Wen, J.; Tian, R.; Zhang, Y.; Jiang, L.; et al. Structure remodeling of soy protein-derived amyloid fibrils mediated by epigallocatechin-3-gallate. *Biomaterials* **2022**, *283*, 121455. [[CrossRef](#)]
28. Jung, J.-M.; Savin, G.; Pouzot, M.; Schmitt, C.; Mezzenga, R. Structure of Heat-Induced β -Lactoglobulin Aggregates and their Complexes with Sodium-Dodecyl Sulfate. *Biomacromolecules* **2008**, *9*, 2477–2486. [[CrossRef](#)] [[PubMed](#)]
29. Cheong, D.Y.; Lee, W.; Park, I.; Park, J.; Lee, G. Amyloid Formation in Nanoliter Droplets. *Int. J. Mol. Sci.* **2022**, *23*, 5480. [[CrossRef](#)]
30. Cheong, D.Y.; Roh, S.; Park, I.; Lin, Y.; Lee, Y.-H.; Lee, T.; Lee, S.W.; Lee, D.; Jung, H.G.; Kim, H.; et al. Proteolysis-driven proliferation and rigidification of pepsin-resistant amyloid fibrils. *Int. J. Biol. Macromol.* **2023**, *227*, 601–607. [[CrossRef](#)] [[PubMed](#)]
31. Wang, S.T.; Lin, Y.; Spencer, R.K.; Thomas, M.R.; Nguyen, A.I.; Amdursky, N.; Pashuck, E.T.; Skaalure, S.C.; Song, C.Y.; Parmar, P.A.; et al. Sequence-Dependent Self-Assembly and Structural Diversity of Islet Amyloid Polypeptide-Derived β -Sheet Fibrils. *ACS Nano* **2017**, *11*, 8579–8589. [[CrossRef](#)]
32. Northrop, J.H. Crystalline Trypsin: IV. Reversibility of the Inactivation and Denaturation of Trypsin by Heat. *J. Gen. Physiol.* **1932**, *16*, 323–337. [[CrossRef](#)]
33. Cai, J.; Jin, T.; Kou, J.; Zou, S.; Xiao, J.; Meng, Q. Lucas–Washburn Equation-Based Modeling of Capillary-Driven Flow in Porous Systems. *Langmuir* **2021**, *37*, 1623–1636. [[CrossRef](#)] [[PubMed](#)]
34. Escobedo, C.; Sinton, D. Microfluidic liquid actuation through ground-directed electric discharge. *Microfluid. Nanofluidics* **2011**, *11*, 653–662. [[CrossRef](#)]
35. Perez-Cruz, A.; Stiharu, I.; Dominguez-Gonzalez, A. Two-dimensional model of imbibition into paper-based networks using Richards’ equation. *Microfluid. Nanofluidics* **2017**, *21*, 98. [[CrossRef](#)]
36. Camplisson, C.K.; Schilling, K.M.; Pedrotti, W.L.; Stone, H.A.; Martinez, A.W. Two-ply channels for faster wicking in paper-based microfluidic devices. *Lab A Chip* **2015**, *15*, 4461–4466. [[CrossRef](#)]
37. Stepanenko, O.V.; Sulatsky, M.I.; Mikhailova, E.V.; Stepanenko, O.V.; Kuznetsova, I.M.; Turoverov, K.K.; Sulatskaya, A.I. Trypsin Induced Degradation of Amyloid Fibrils. *Int. J. Mol. Sci.* **2021**, *22*, 4828. [[CrossRef](#)] [[PubMed](#)]
38. Numata, K.; Kaplan, D.L. Mechanisms of enzymatic degradation of amyloid Beta microfibrils generating nanofilaments and nanospheres related to cytotoxicity. *Biochemistry* **2010**, *49*, 3254–3260. [[CrossRef](#)]
39. Greca, L.G.; De France, K.J.; Majoinen, J.; Kummer, N.; Luotonen, O.I.V.; Campioni, S.; Rojas, O.J.; Nyström, G.; Tardy, B.L. Chitin–amyloid synergism and their use as sustainable structural adhesives. *J. Mater. Chem. A* **2021**, *9*, 19741–19753. [[CrossRef](#)]
40. Shimanovich, U.; Efimov, I.; Mason, T.O.; Flagmeier, P.; Buell, A.K.; Gedanken, A.; Linse, S.; Åkerfeldt, K.S.; Dobson, C.M.; Weitz, D.A.; et al. Protein microgels from amyloid fibril networks. *ACS Nano* **2015**, *9*, 43–51. [[CrossRef](#)]
41. Adamcik, J.; Jung, J.-M.; Flakowski, J.; De Los Rios, P.; Dietler, G.; Mezzenga, R. Understanding amyloid aggregation by statistical analysis of atomic force microscopy images. *Nat. Nanotechnol.* **2010**, *5*, 423–428. [[CrossRef](#)] [[PubMed](#)]
42. Khanna, S.; Singh, A.K.; Behera, S.P.; Gupta, S. Thermoresponsive BSA hydrogels with phase tunability. *Mater. Sci. Eng. C* **2021**, *119*, 111590. [[CrossRef](#)]
43. Lee, T.; Kim, I.; Cheong, D.Y.; Roh, S.; Jung, H.G.; Lee, S.W.; Kim, H.S.; Yoon, D.S.; Hong, Y.; Lee, G. Selective colorimetric urine glucose detection by paper sensor functionalized with polyaniline nanoparticles and cell membrane. *Anal. Chim. Acta* **2021**, *1158*, 338387. [[CrossRef](#)] [[PubMed](#)]
44. Lee, T.; Kim, C.; Kim, J.; Seong, J.B.; Lee, Y.; Roh, S.; Cheong, D.Y.; Lee, W.; Park, J.; Hong, Y.; et al. Colorimetric Nanoparticle-Embedded Hydrogels for a Biosensing Platform. *Nanomaterials* **2022**, *12*, 1150. [[CrossRef](#)]
45. Lee, T.; Lee, H.-T.; Hong, J.; Roh, S.; Cheong, D.Y.; Lee, K.; Choi, Y.; Hong, Y.; Hwang, H.-J.; Lee, G. A regression-based machine learning approach for pH and glucose detection with redox-sensitive colorimetric paper sensors. *Anal. Methods* **2022**, *14*, 4749–4755. [[CrossRef](#)]
46. Tsiatsiani, L.; Heck, A.J.R. Proteomics beyond trypsin. *FEBS J.* **2015**, *282*, 2612–2626. [[CrossRef](#)] [[PubMed](#)]
47. Gershon, P.D. Cleaved and Missed Sites for Trypsin, Lys-C, and Lys-N Can Be Predicted with High Confidence on the Basis of Sequence Context. *J. Proteome Res.* **2014**, *13*, 702–709. [[CrossRef](#)] [[PubMed](#)]

48. Patari, S.; Mahapatra, P.S. Liquid Wicking in a Paper Strip: An Experimental and Numerical Study. *ACS Omega* **2020**, *5*, 22931–22939. [[CrossRef](#)]
49. Koursari, N.; Arjmandi-Tash, O.; Trybala, A.; Starov, V.M. Drying of Foam under Microgravity Conditions. *Microgravity Sci. Technol.* **2019**, *31*, 589–601. [[CrossRef](#)]
50. Seabra, I.; Gil, H. Cotton gauze bandage: A support for protease immobilization for use in biomedical applications. *Rev. Bras. Cienc. Farm.* **2007**, *43*, 535–542. [[CrossRef](#)]

Disclaimer/Publisher’s Note: The statements, opinions and data contained in all publications are solely those of the individual author(s) and contributor(s) and not of MDPI and/or the editor(s). MDPI and/or the editor(s) disclaim responsibility for any injury to people or property resulting from any ideas, methods, instructions or products referred to in the content.